Journal of Sound and Vibration (2000) **232**(4), 807–822
doi:10.1006/jsvi.1999.2787, available online at http://www.idealibrary.com on IDEAL®

VIBRATION ANALYSIS OF ANNULAR PLATES USING MODE SUBTRACTION METHOD

W. O. WONG, L. H. YAM, Y. Y. LI, L. Y. LAW AND K. T. CHAN

Department of Mechanical Engineering, The Hong Kong Polytechnic University, Hung Hom, Kowloon, Hong Kong

(*Received* 3 *September* 1999, *and in final form* 13 *November* 1999)

In this paper, a mode subtraction method is presented to investigate the sensitivity of changes in displacement mode shape of annular plates relative to the hole size. It is proved that the displacement modes are sensitive to the presence of a hole in a plate. Jump phenomena are observed in the "residual mode shape", and the number and locations of peaks are determined based upon the displacement modal analysis. Numerical analyses of the changes in displacement mode shapes for different boundary conditions (C–F, S–F, F–F) and relative hole sizes are given. Experimental tests show good agreement with the numerical results.

1. INTRODUCTION

The annular plate is one of the most popular kinds of components used in mechanical and structural engineering, and the complicated dynamic characteristics and vibration analyses of annular plates have been the focus of research efforts [1–3]. Usually, natural frequencies and mode shapes are the major parameters for vibration analysis of annular plates, and fruitful results have been presented for years [4–7]. In recent years, most researchers have investigated the dynamic behaviours at the circumference of the hole for different structures using the strain modal analysis, and verified that strain mode is sensitive to the local changes of structures, while displacement mode is not [8–10].

Since both the strain mode and displacement mode are intrinsic dynamic characteristics of a structure and correspond to each other, research of the vibration behaviour at the circumference of the hole in annular plates using displacement modal analysis is of great interest. Literature surveys show that although some investigators have discussed the changes at the damaged region of a beam, they believe that changes in the displacement mode shapes are not localized to the damaged region [11]. For annular plates, no one has reported results on this aspect in detail.

Based on this consideration, the present work describes the theoretical and computational aspects of the mode subtraction method in analyzing the vibration behaviours at the circumference of the hole in annular plates with three types of boundary conditions: clamped–free (C–F), simply supported–free (S–F) and free–free (F–F). The differences in the normalized displacement mode shapes are derived, and the number and locations of peaks at the circumference of the hole are discussed. Then, numerical results and experimental tests are given to indicate the effectiveness of the method presented for vibration analysis of annular plates. Finally, some conclusions are drawn.

0022-460X/00/190807 + 16 $35.00/0

2. FORMULATION AND SOLUTION

The equation of motion of an annular plate with polar co-ordinates (r, θ) is given by [12]

$$D\nabla^4 w(r, \theta, t) + \rho h \frac{\partial^2 w(r, \theta, t)}{\partial t^2} = 0, \quad c \leqslant r < a, \tag{1}$$

where

$$\nabla^2 = \frac{\partial^2}{\partial r^2} + \frac{1}{r}\frac{\partial}{\partial r} + \frac{1}{r^2}\frac{\partial^2}{\partial \theta^2}.$$

w, D, ρ and h are the transverse deflection, flexural rigidity, density and thickness of the plate respectively. c and a are the radii of the hole and the plate respectively. Based on the vibration analysis of plate and mode superposition theory, the solution of equation (1) can be approached using

$$w(r, \theta, t) = \sum_{n=0}^{\infty} W_n(r, \theta)\, \mathrm{e}^{\mathrm{i}pt}, \tag{2}$$

where $W_n(r, \theta)$ is the mode shape function expressed as [4]

$$W_n(r, \theta) = [A_{1n}\mathrm{J}_n(kr/a) + A_{2n}\mathrm{J}_n(\mathrm{i}kr/a) + A_{3n}\mathrm{Y}_n(kr/a) + A_{4n}\mathrm{H}_n(\mathrm{i}kr/a)]\, \mathrm{e}^{\mathrm{i}(n\theta + \alpha)}. \tag{3}$$

In equations (2) and (3), p is the circular frequency of natural vibration in radians per second. J_n, Y_n and H_n are the Bessel function of the first kind, the second kind and the Hankel function of the first kind of order n, respectively, $(A_{1n}, A_{2n}, A_{3n}, A_{4n})$ are the coefficients, $k = a(p^2\rho h/D)^{1/4}$ is the frequency parameter, and α a constant related to the orientation of the mode shape.

Equation (2) contains the information of circular frequency p and mode shape $W_n(r, \theta)$ for the annular plate. Detailed solutions of the coefficients $A_{in}(i = 1, \ldots, 4)$ of Bessel function in determining the mode shapes functions expressed as equation (3) for three common types of boundary conditions are given in Appendix A.

In order to investigate the vibration behaviour at the circumference of the hole in an annular plate, a mode subtraction process, which evaluates the relative change of the same order normalized mode shapes of plates with $c/a \neq 0$ and $c/a = 0$, is studied analytically and presented later.

Consider an annular plate with a free inner edge $(c/a \neq 0)$ vibration at the nth normal mode. The bending moment of the plate can be expressed as [13]

$$M_n(r, \theta) = D\left\{\frac{\partial^2 W_n(r, \theta)}{\partial r^2} + \nu\left[\frac{1}{r}\frac{\partial W_n(r, \theta)}{\partial r} + \frac{1}{r^2}\frac{\partial^2 W_n(r, \theta)}{\partial \theta^2}\right]\right\}, \tag{4}$$

where ν is the Possion ratio. Obviously, the bending moment at the free inner edge of the plate must be zero, i.e., $M_n(r, \theta)|_{r=c} = 0$. Applying some manipulations to equation (4), the curvature of the normalized displacement mode along radial direction can be expressed as [13]

$$\frac{\partial^2 \bar{W}_n(r, \theta)}{\partial r^2} = -\nu\left(\frac{1}{r}\frac{\partial \bar{W}_n(r, \theta)}{\partial r} + \frac{1}{r^2}\frac{\partial^2 \bar{W}_n(r, \theta)}{\partial \theta^2}\right). \tag{5}$$

For the case of $c/a = 0$ (a circular plate without hole), the bending moment $M_{no}(r, \theta)$ satisfies

$$M_{no}(r, \theta) = D\left\{\frac{\partial^2 W_{no}(r, \theta)}{\partial r^2} + v\left[\frac{1}{r}\frac{\partial^2 W_{no}(r, \theta)}{\partial r} + \frac{1}{r^2}\frac{\partial^2 W_{no}(r, \theta)}{\partial \theta^2}\right]\right\}. \tag{6}$$

Since $M_{no}(r, \theta)$ at $r = c$ is generally not equal to zero, let

$$\varphi(\theta) = \left.\frac{\partial^2 W_{no}(r, \theta)}{\partial r^2}\right|_{r=c} + \frac{v}{c}\left.\frac{\partial^2 W_{no}(r, \theta)}{\partial r}\right|_{r=c} + \frac{v}{c^2}\frac{\partial^2 W_{no}(c, \theta)}{\partial \theta^2}. \tag{7}$$

The corresponding curvature of the normalized displacement mode can be expressed as

$$\frac{\partial^2 \bar{W}_{no}(r, \theta)}{\partial r^2} = -v\left(\frac{1}{r}\frac{\partial^2 \bar{W}_{no}(r, \theta)}{\partial r} + \frac{1}{r^2}\frac{\partial^2 \bar{W}_{no}(r, \theta)}{\partial \theta^2}\right) + \varphi(\theta). \tag{8}$$

In equation (8), $\bar{W}_{no}(r, \theta)$ is the nth normalized mode shape of a circular plate expressed as

$$\bar{W}_{no}(r, \theta) = [A_{1no} \mathrm{J}_n(kr/a) + A_{2no} \mathrm{J}_n(\mathrm{i}kr/a)]\, \mathrm{e}^{\mathrm{i}(n\theta + \alpha)}. \tag{9}$$

Then the difference in curvature between the same order normalized displacement modes of a circular plate and of an annular plate is

$$\begin{aligned}
\Delta \bar{W}_n''(r, \theta) &= \frac{\partial^2 \bar{W}_{no}(r, \theta)}{\partial r^2} - \frac{\partial^2 \bar{W}_n(r, \theta)}{\partial r^2} \\
&= -v\left[\frac{1}{r}\left(\frac{\partial \bar{W}_{no}(r, \theta)}{\partial r} - \frac{\partial \bar{W}_n(r, \theta)}{\partial r}\right) + \frac{1}{r^2}\left(\frac{\partial^2 \bar{W}_{no}(r, \theta)}{\partial \theta^2} - \frac{\partial^2 \bar{W}_n(r, \theta)}{\partial \theta^2}\right)\right] + \varphi(\theta) \\
&= \frac{v}{r}\left\{(A_{1n} - A_{1no})\left[\mathrm{J}_n'(kr/a) - \frac{n^2}{r}\mathrm{J}_n(kr/a)\right]\right. \\
&\quad + (A_{2n} - A_{2no})\left[\mathrm{J}_n'(\mathrm{i}kr/a) - \frac{n^2}{r}\mathrm{J}_n(\mathrm{i}kr/a)\right] \\
&\quad \left. + A_{3n}\left[\mathrm{Y}_n'(kr/a) - \frac{n^2}{r}\mathrm{Y}_n(kr/a)\right] + A_{4n}\left[\mathrm{H}_n'(\mathrm{i}kr/a) - \frac{n^2}{r}\mathrm{H}_n(\mathrm{i}kr/a)\right]\right\} \\
&\quad \times \mathrm{e}^{\mathrm{i}(n\theta + \alpha)} + z\varphi(\theta).
\end{aligned} \tag{10}$$

Equation (10) can be rewritten as

$$\Delta \bar{W}_n''(r, \theta) = \psi(n)\, \mathrm{e}^{\mathrm{i}(n\theta + \alpha)} + \varphi(\theta), \quad n = 0, 1, 2, \ldots, \tag{11}$$

where

$$\psi(n) = \frac{v}{r}\left\{(A_{1n} - A_{1no})\left[\mathrm{J}'_n(kr/a) - \frac{n^2}{r}\mathrm{J}_n(kr/a)\right] + (A_{2n} - A_{2no})\left[\mathrm{J}'_n(\mathrm{i}kr/a) - \frac{n^2}{r}\mathrm{J}_n(\mathrm{i}kr/a)\right]\right.$$
$$\left. + A_{3n}\left[\mathrm{Y}'_n(kr/a) - \frac{n^2}{r}\mathrm{Y}_n(kr/a)\right] + A_{4n}\left[\mathrm{H}'_n(\mathrm{i}kr/a) - \frac{n^2}{r}\mathrm{H}_n(\mathrm{i}kr/a)\right]\right\}, \tag{12}$$
$$n = 0, 1, 2, \ldots$$

Integrating equation (10) twice leads to

$$\begin{aligned}\Delta\bar{W}_n(r,\theta) &= \bar{W}_{no}(r,\theta) - \bar{W}_n(r,\theta)\\ &= v\left\{(A_{1n} - A_{1no})\int\left[\int\left(\frac{1}{r}\mathrm{J}'_n(kr/a) - \frac{n^2}{r^2}\mathrm{J}_n(kr/a)\right)\mathrm{d}r\right]\mathrm{d}r + (A_{no} - A_{2no})\right.\\ &\quad\times\int\left[\int\left(\frac{1}{r}\mathrm{J}'_n(\mathrm{i}kr/a) - \frac{n^2}{r^2}\mathrm{J}_n(\mathrm{i}kr/a)\right)\mathrm{d}r\right]\mathrm{d}r\\ &\quad + A_{3n}\int\left[\int\left(\frac{1}{r}\mathrm{Y}'_n(kr/a) - \frac{n^2}{r^2}\mathrm{Y}_n(kr/a)\right)\mathrm{d}r\right]\mathrm{d}r\\ &\quad\left. + A_{4n}\int\left[\int\left(\frac{1}{r}H'_n(\mathrm{i}kr/a) - \frac{n^2}{r^2}\mathrm{H}_n(\mathrm{i}kr/a)\right)\mathrm{d}r\right]\mathrm{d}r\right\}\mathrm{e}^{\mathrm{i}(n\theta+\alpha)} + \frac{1}{2}\varphi(\theta)r^2,\end{aligned} \tag{13}$$

when $r = c$. The change of the same order-displacement mode, which is defined as the residual mode shape, is given by

$$\begin{aligned}\iint \Delta\bar{W}''_n(r,\theta)\,\mathrm{d}r\,\mathrm{d}r|_{r=c} &= \Delta\bar{W}_n(c,\theta) = \bar{W}_{no}(c,\theta) - \bar{W}_n(c,\theta)\\ &\qquad\qquad n = 0, 1, 2, \ldots,\\ &= \chi(n)\,\mathrm{e}^{\mathrm{i}(n\theta+\alpha)} + \tfrac{1}{2}\varphi(\theta)c^2,\end{aligned} \tag{14}$$

where

$$\begin{aligned}\chi(n) = v\left\{\right.&(A_{1n} - A_{1no})\int_c\left[\int\left(\frac{n^2}{r^2}\mathrm{J}_n(kr/a) - \frac{1}{r}\mathrm{J}'_n(kr/a)\right)\mathrm{d}r\right]\mathrm{d}r\Big|_{r=c}\\ &+ (A_{2n} - A_{2no})\int_c\left[\int\left(\frac{n^2}{r^2}\mathrm{J}_n(\mathrm{i}kr/a) - \frac{1}{r}\mathrm{J}'_n(\mathrm{i}kr/a)\right)\mathrm{d}r\right]\mathrm{d}r\Big|_{r=c}\\ &+ A_{3n}\int_c\left[\int\left(\frac{n^2}{r^2}\mathrm{Y}_n(kr/a) - \frac{1}{r}\mathrm{Y}'_n(kr/a)\right)\mathrm{d}r\right]\mathrm{d}r\Big|_{r=c}\\ &\left.+ A_{4n}\int_c\left[\int\left(\frac{n^2}{r^2}\mathrm{H}_n(\mathrm{i}kr/a) - \frac{1}{r}\mathrm{H}'_n(\mathrm{i}kr/a)\right)\mathrm{d}r\right]\mathrm{d}r\Big|_{r=c}\right\},\end{aligned} \tag{15}$$

$\Delta\bar{W}_n(c,\theta)$ depends on parameters (θ, n). The real part of $\Delta\bar{W}_n(c,\theta)$ represents the change in mode shapes. In this case, peaks will occur at the locations where

$$\Re e\left[\frac{\partial(\Delta\bar{W}_n(c,\theta))}{\partial\theta}\right] = 0. \tag{16}$$

$\mathfrak{R}e$ stands for the real part of the corresponding function. From equation (7), $\varphi(\theta)$ can be expressed as $\varphi(\theta) = \eta(n)\,e^{i(n\theta + \alpha)}$. Without loss of generality, denote

$$\chi(n) = \chi_R(n) + i\chi_I(n), \quad \eta(n) = \eta_R(n) + i\eta_I(n). \tag{17}$$

By substituting equation (17) into equation (14) and differentiating with respect to θ, equation (16) can be rewritten as

$$-n\left\{\left[\chi_R(n) + \frac{c^2}{2}\eta_R(n)\right]\sin(n\theta + \alpha) + \left[\chi_I(n) + \frac{c^2}{2}\eta_I(n)\right]\cos(n\theta + \alpha)\right\} = 0, \tag{18}$$

i.e.,

$$\theta = \frac{1}{n}\left(-\operatorname{arctg}\frac{2\chi_I(n) + c^2\eta_I(n)}{2\chi_R(n) + c^2\eta_R(n)} - \alpha\right), \quad n \neq 0. \tag{19}$$

From the above analysis, the following can be observed:

- In equation (14), changes increase significantly with the increase of c.
- In the case of $n = 0$, i.e., the first mode, $\Delta\bar{W}_n(c, \theta) = \chi(0)\,e^{i\alpha} + \frac{1}{2}\varphi c^2$. That is to say, when θ varies from 0 to 2π, $\Delta\bar{W}_n(c, \theta)$ retains the same value. This means that only one peak appeared around the hole.
- In the case of $n \neq 0$, peaks can be observed at those locations where equation (19) can be satisfied, and the number of peaks is equal to $2n$. For example, there are two peaks for the second mode ($n = 1$), and four peaks for the third mode ($n = 2$).
- Changes at the circumference of the hole would be observed using displacement modal analysis, i.e., the residual displacement mode is sensitive to the discontinuity of structures.

3. NUMERICAL RESULTS

To verify the theoretical prediction in the previous section, the vibrations of an annular plate are analyzed for different boundary conditions and hole size (c/a) ratios. According to equation (A4), the frequency parameter k can be solved and listed in Table 1. The coefficients (A_{1n}, A_{2n}, A_{3n}, A_{4n}) in determining mode shapes are solved by equations (A5), (A7), (A9), respectively, and the displacement modes are identified using equation (3) and normalized by dividing the whole set of deflections by the maximum value.

TABLE 1

Frequency parameter k ($\nu = \frac{1}{3}$)

		c/a Ratio				
Case	Mode	0	0·05	0·1	0·2	0·4
C–F	(1, 0)	4·610	4·609	4·603	4·526	4·403
	(2, 0)	5·905	5·898	5·878	5·811	5·598
S–F	(1, 0)	3·733	3·732	3·729	3·685	3·450
	(2, 0)	5·064	5·059	5·044	4·993	4·806
F–F	(2, 0)	2·291	2·288	2·280	2·247	2·128
	(3, 0)	3·549	3·495	3·495	3·490	3·430

Figures 1(a) and 1(b) show the normalized displacement modes of the C–F annular plate with $c/a = 0$ and $c/a = 0{\cdot}1$ respectively. Comparison of Figures 1(a) and 1(b) shows that the same order mode shapes are nearly the same, i.e., no obvious change can be found. However, after subtraction of one mode shape from the other, some obvious changes can be observed at the circumference of the hole. The residual mode shapes of the same order displacement modes are plotted in the form of mesh and contour curves in Figure 1(c). It can be found that the maximum differences occur around the hole, whereas changes are trivial outside the hole, and two peaks appear in mode (1,0) and four in mode (2,0).

Figures 2(a) and 2(b) give the residual mode shapes of the C–F annular plate with different c/a ratios for modes (1,0) and (2,0) respectively. When the c/a ratio is decreased from 0·2 to 0·05, the amplitudes of changes decrease correspondingly, but peaks can still be observed around the hole. It means that although the peaks of the residual mode shape for annular plates with a larger hole is more dramatic than that in the case with a small hole, peaks occur even for a very small hole. This phenomenon gives us some clues on damage detection for circular plates.

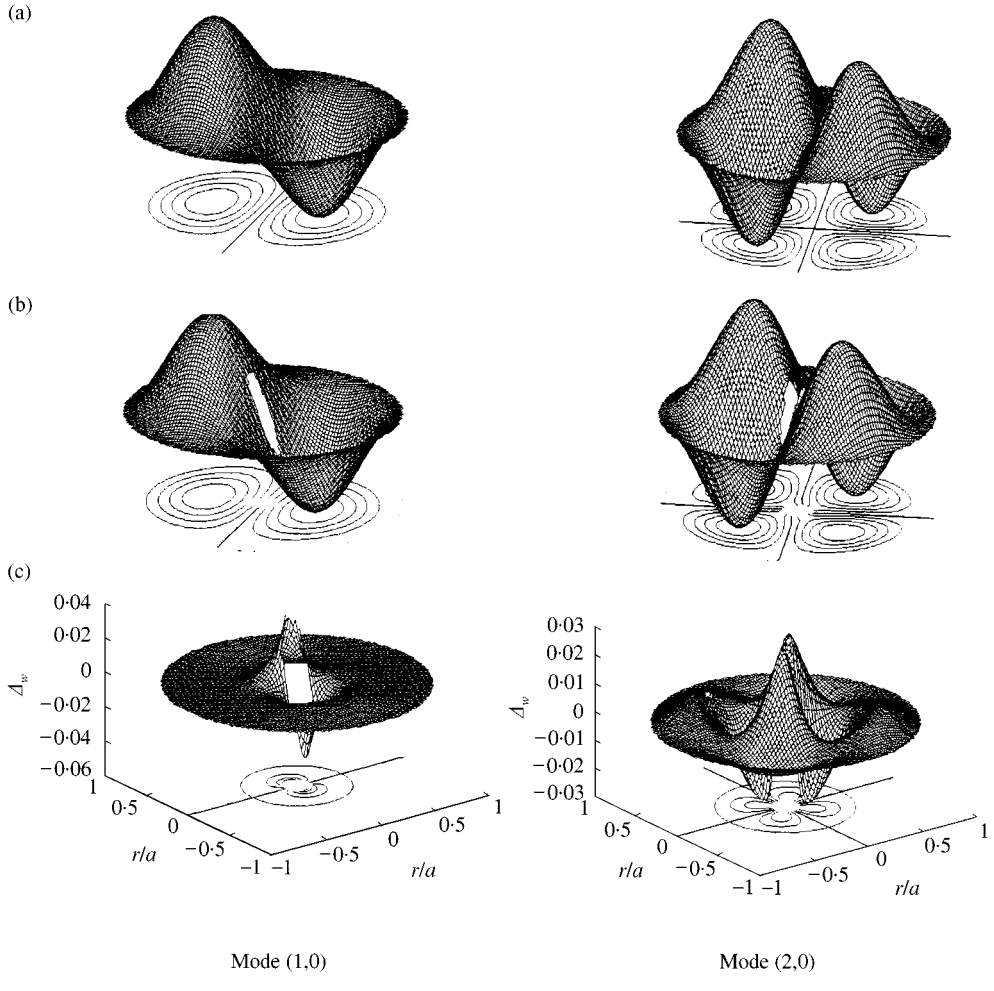

Figure 1. Displacement mode shapes of the C–F annular plate for modes (1,0) and (2,0). (a) $c/a = 0$; (b) $c/a = 0{\cdot}1$; (c) (a)–(b).

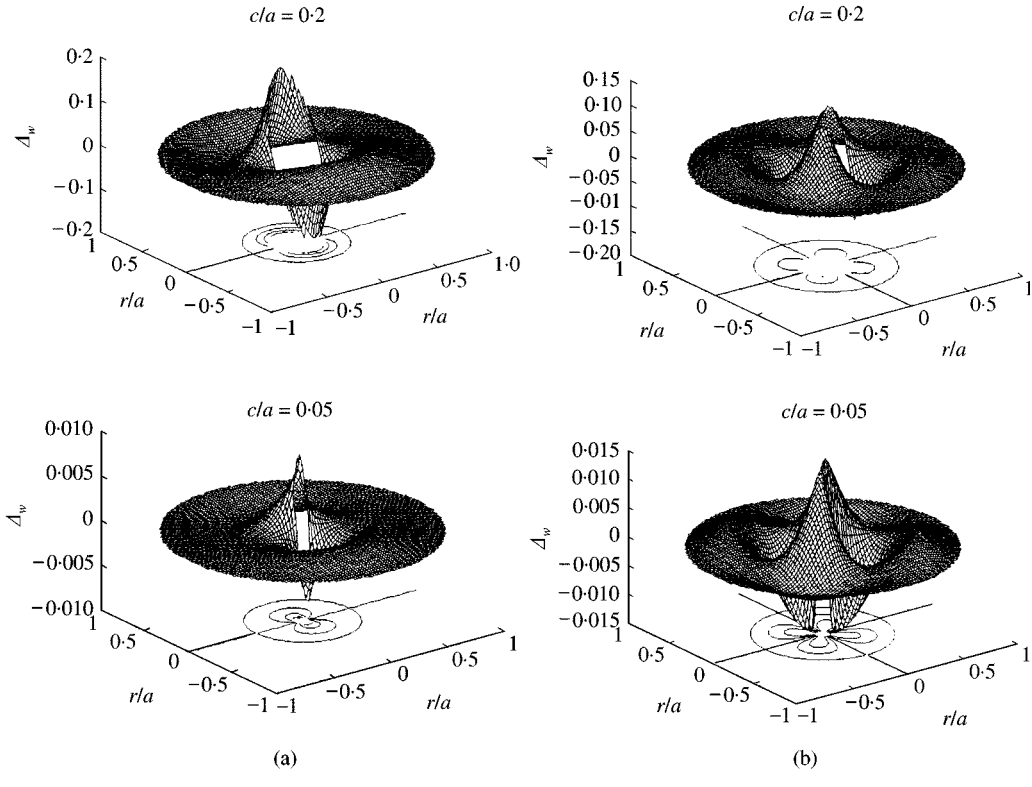

Figure 2. Residual mode shapes of the C–F annular plate with $c/a = 0{\cdot}2$ and 0·05. (a) mode (1,0); (b) mode (2,0).

The displacement mode shapes and residual mode shapes for the S–F and F–F annular plates are plotted in Figures 3–6, and similar results have been obtained. In Figure 5, since the first two modes ((0, 0) and (1, 0)) correspond to the rigid-body translation and rotation for the F–F plate, modes (2,0) and (3,0) are selected for discussion.

From Figures 1–4, it can be seen that a node circle appeared at the same location in the difference mode shape even though it did not in the normal displacement mode shape. The reason is that the difference mode shape given by equation (13) can be expressed as the function of r and the node circle will appear at those locations where $\Delta\bar{W}_n(r, \theta) = 0$ is satisfied. Obviously, if vibration sensors are located at the node circle of $\Delta\bar{W}_n(r, \theta)$, no change in displacement mode can be obtained. It would help the determination of sensor locations during measurement.

It should be pointed out that when the dimension of a hole equals the dimension of a nodal circle, no peak can be observed using the mode subtraction method. Figure 7 shows the residual mode shapes of the S–F annular plate with $c/a = 0.4$. In Figure 7(a), since the hole overlaps with the nodal circle exactly, no peak is found around the hole for mode(1,0). Two peaks are observed in the case of $c/a = 0{\cdot}2$ as shown in Figure 4(a). Figure 7(b) is for mode (2,0), and four peaks are clearly observed.

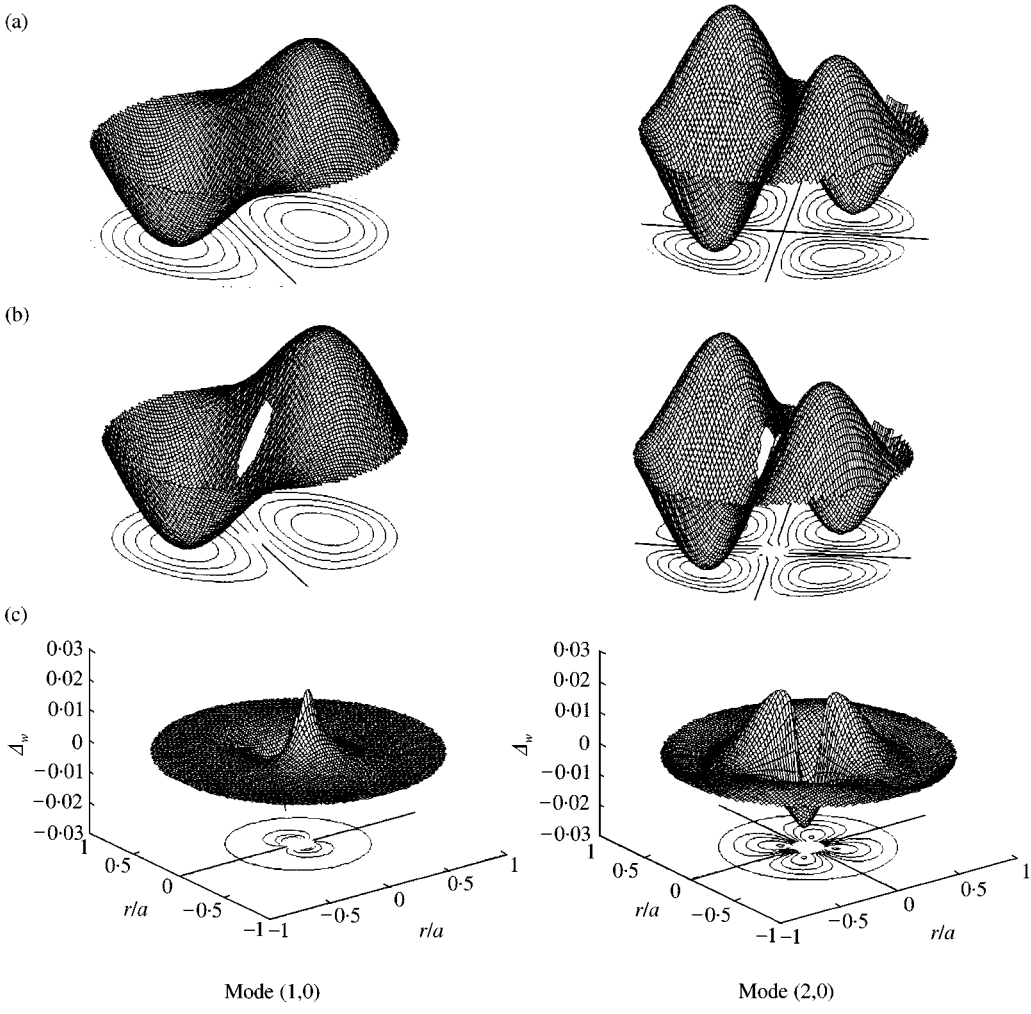

Figure 3. Displacement mode shapes of the S–F annular plate for modes (1,0) and (2,0). (a) $c/a = 0$; (b) $c/a = 0{\cdot}1$; (c) (a)–(b).

4. EXPERIMENTAL ANALYSIS

In this section, experimental tests in a vibration analysis of mode (1,0) for the C–F annular plate have been carried out. The parameters of the thin steel plate are: $a = 70$ mm, $h = 0{\cdot}2$ mm, $E = 200$ GPa, $\rho = 7800$ kg/m^3, $v = 0{\cdot}3$ and $c/a = 0{\cdot}2$. The schematic diagram of the experimental set-up is shown in Figure 8. An excitation signal was generated by a B&K 3023 signal analyzer, then amplified by a B&K 2706 power amplifier, and exerted on the plate through the B&K 4810 exciter. The force was measured by a B&K 8203 transducer fixed between the flexible string and the exciter, and the vibration responses were sensed by the B&K 4397 accelerometers at five different locations on the plate.

In general, the actuator is assigned at the location of the anti-node to ensure that enough input energy is provided to the structure, and the accelerometers are located at those positions where the peaks appear. To determine these locations properly, the following

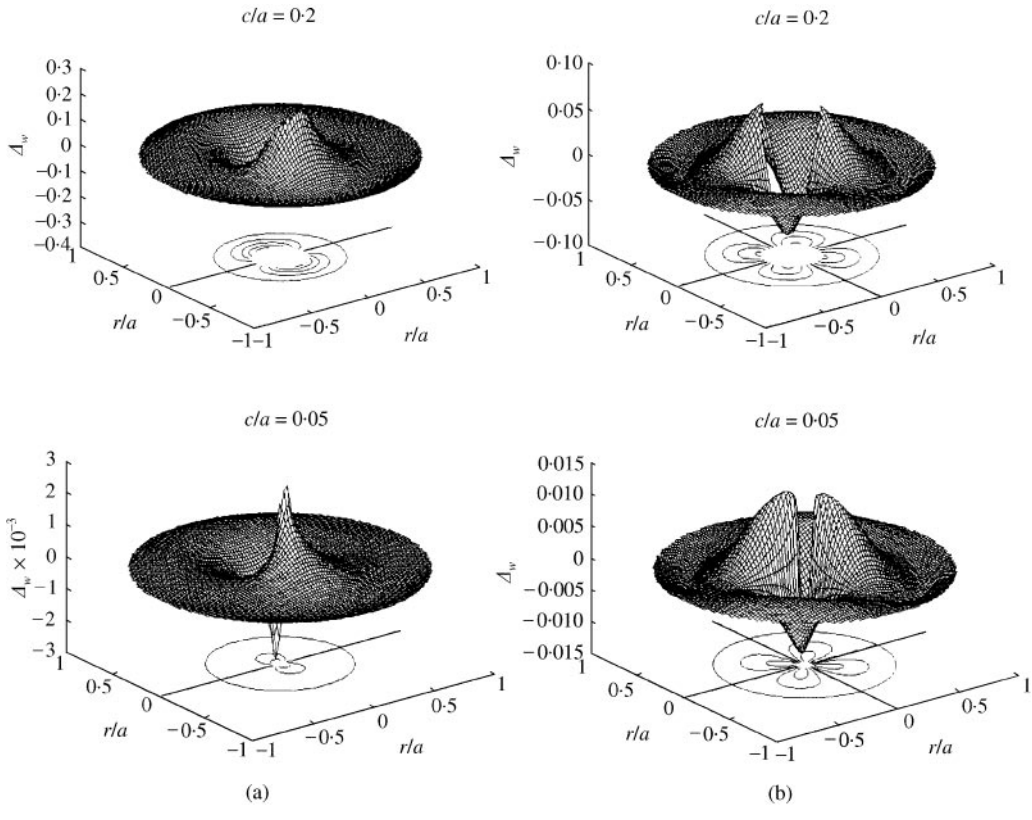

Figure 4. Residual mode shapes of the S–F annular plate with $c/a = 0{\cdot}2$ and 0·05. (a) mode (1,0); (b) mode (2,0).

procedures were adopted: firstly, the accelerometers were placed randomly to find the nodal line (Figure 9, line L_1). For mode (1,0), the cross-section of the anti-nodes will be perpendicular to the nodal line, and it is 40% away from the central point. The accelerometers were then set at locations $(s_1, s_3, s_4, s_5, s_6)$ as shown in Figure 9, and the actuator at the point of the anti-node s_2 marked in the figure.

In order to investigate the vibration around the hole, tests for the cases of $c/a = 0$ and $c/a = 0{\cdot}2$ were done, and the FRFs at points $(s_1, s_3, s_4, s_5, s_6)$ were recorded by an FFT analyzer. The amplitudes at $\omega = 209{\cdot}5$ Hz (with respect to mode (1,0)) for these measuring points were normalized, and the differences of these two cases were calculated. Figure 10 shows the simulation (at cross section) and experimental results of the residual mode shape for the C–F annular plate with $c/a = 0{\cdot}2$. In this figure, two peaks are observed, i.e., $-0{\cdot}133$ at $r/a = -0{\cdot}2\,(s_4)$ and 0·141 at $r/a = 0{\cdot}2(s_3)$, while at other locations (s_1, s_5, s_6), no obvious changes were found. Obviously, good agreement is achieved between the simulation and experiment. It means that significant changes can be detected at the circumference of the hole.

5. CONCLUSION

Vibration analyses of annular plates under different boundary conditions and relative hole sizes are presented. Significant changes at the circumference of the hole can be detected

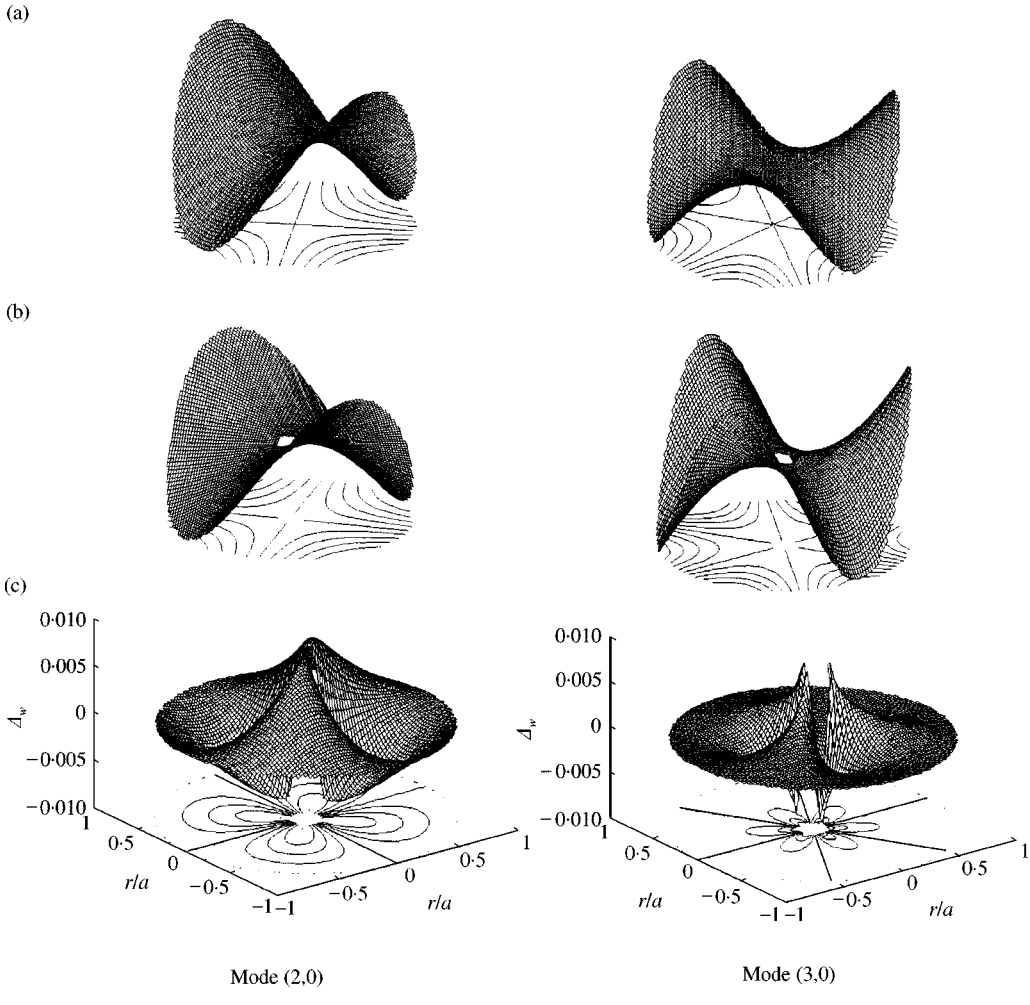

Figure 5. Displacement mode shapes of the F–F annular plate for modes (2,0) and (3,0). (a) $c/a = 0$; (b) $c/a = 0{\cdot}1$; (c) (a)–(b).

by the residual mode shapes, which are characterized using the displacement mode subtraction method. Analytical and numerical results show that even for a small c/a ratio, the jump phenomena around the hole exist, and the number and locations of peaks can be determined. Good agreement is found between the numerical simulations and the experimental tests. It provides a guidance on vibration analysis and measurement for annular plates, and the method may be applied to damage detection of circular plates.

ACKNOWLEDGMENT

The authors would like to thank the Research Committee of The Hong Kong Polytechnic University for the financial support of this project.

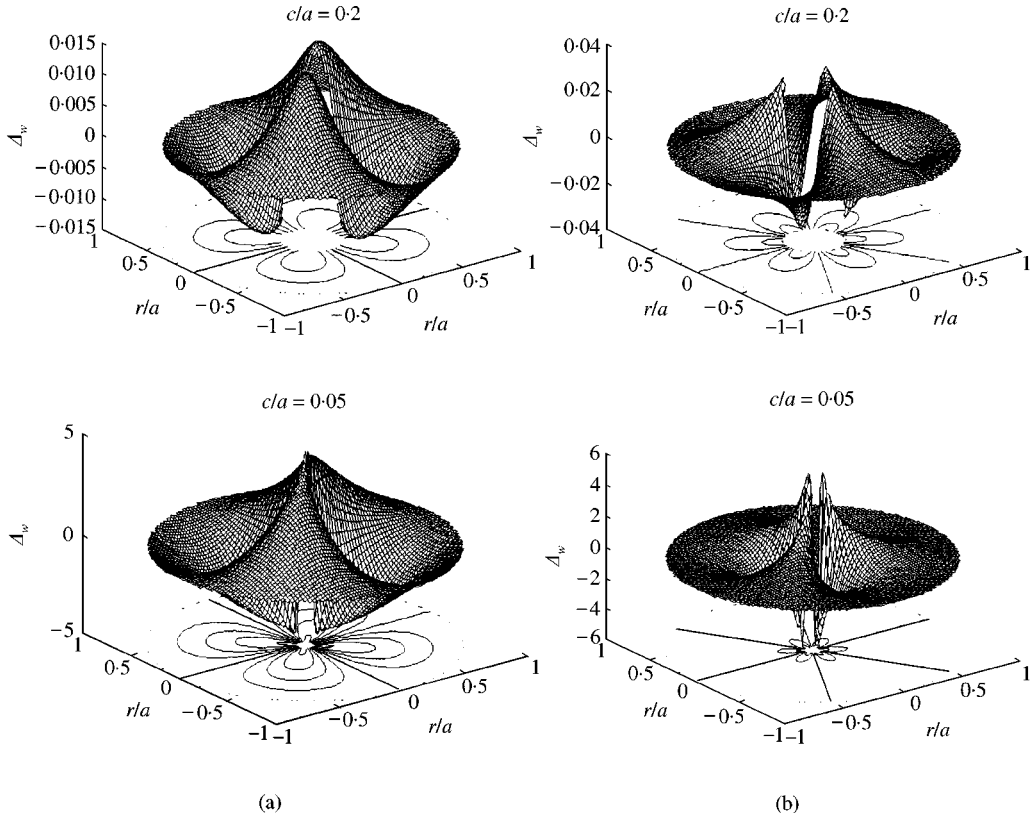

Figure 6. Residual mode shapes of the F–F annular plate with $c/a = 0{\cdot}2$ and 0·05. (a) mode (2,0); (b) mode (3,0).

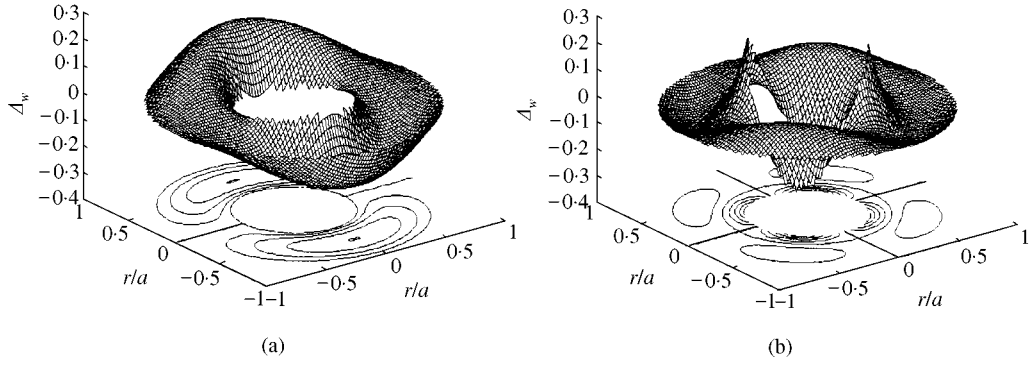

Figure 7. Residual mode shapes of the S–F annular plate with $c/a = 0{\cdot}4$. (a) mode (1,0); (b) mode (2,0).

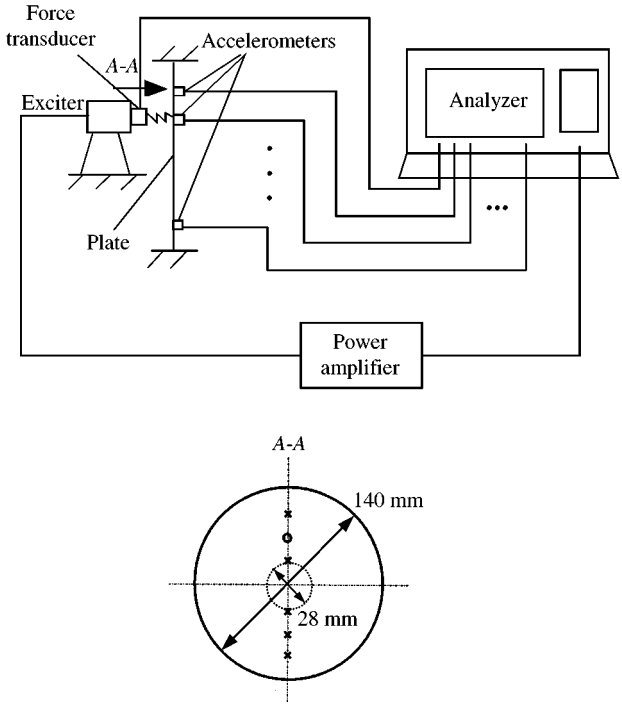

Figure 8. Schematic diagram of the experimental set-up: O —— excitation point; × —— measurement points.

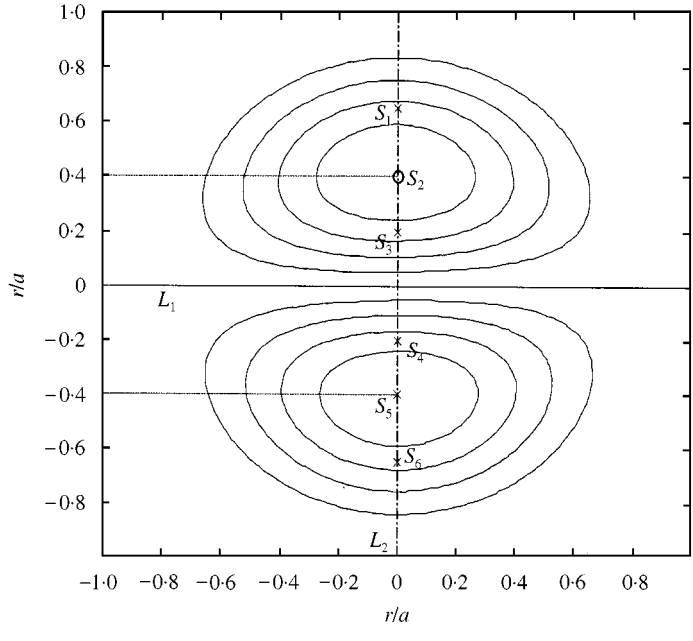

Figure 9. Locations of the nodal line, the anti-nodes and the excitation and measurement points for mode (1,0).

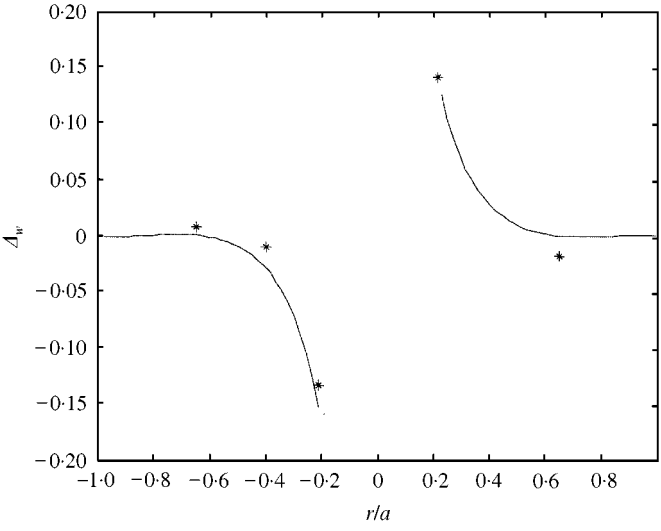

Figure 10. Residual mode shapes of the C–F annular plate with $c/a = 0{\cdot}2$ for mode (1,0): —— simulation result: ∗ experimental result.

REFERENCES

1. V. P. Rangaiah and S. Sadasivan 1981 *Journal of Structural Mechanics* **9**, 211–218. Note on the vibrations of free–free annular plates.
2. W. Karunasena, C. M. Wang, S. Kitipornchai and Y. Xiang 1997 *Computers & Structures* **63**, 455–464. Exact solutions for axisymmetric bending of continuous annular plates.
3. K. Ramesh, D. P. S. Chauhan and A. K. Mallik 1997 *Journal of Sound and Vibration* **206**, 266–274. Free vibration of an annular plate with periodic radical cracks.
4. P. Narayana Raju 1962 *Journal of the Aeronautical Society of India* **14**, 37–52. Vibrations of annular plates.
5. S. M. Vogel and D. W. Skinner 1965 *Journal of Applied Mechanics* **32**, 926–931. Natural frequencies of transversely vibrating uniform annular plates.
6. A. H. Nayfeh, D. T. Mook, D. W. Lobitz and S. Sridhar 1976 *Journal of Sound and Vibration* **47**, 75–84. Vibrations of nearly annular and circular plates.
7. G. Ghen and J. Zhou 1993 Vibration and Damping in Distributed Systems, Vol. II: WKB and Wave Methods, Visualization and Experimentation, 258–264. Boca Raton: CRC Press.
8. O. Bernasconi and D. J. Ewins 1989 *International Journal of Analytical and Experimental Modal Analysis*, **4**, 68–76. Modal strain/stress fields.
9. L. H. Yam, T. P. Leung, D. B. Li and K. Z. Xue 1996 *Journal of Sound and Vibration* **192**, 251–260. Theoretical and experimental study of modal strain analysis.
10. C. F. Liu and Y. T. Lee 1997 *Journal of Sound and Vibration* **208**, 47–54. Axisymmetric straining modes in the vibration of annular plates.
11. A. K. Pandey, M. Biswas and M. M. Samman 1991 *Journal of Sound and vibration* **145**, 321–332. Damage detection from changes in curvature mode shapes.
12. A. W. Leissa 1993 *Vibration of Plates*, 7–35. New York: Published for the Acoustical Society of America through the American Institute of Physics.
13. R. D. Blevins 1979 *Formulas for Natural Frequency and Mode Shape*, 235–240. New York: Van Nostrand Reinhold Co., Litton Educational Publishing Inc.

APPENDIX A. DETAILED SOLUTIONS OF THE COEFFICIENTS $A_{in} (i = 1, \ldots, 4)$

Case 1: Clamped-outer, free-inner (C–F): In this case, the boundary conditions are

$$W_n(r, \theta) = \left.\frac{\partial W_n(r, \theta)}{\partial r}\right|_{r=a} = 0,$$

$$M_n(r, \theta) = V_n(r, \theta)|_{r=c} = 0, \tag{A1}$$

where $M_n(r, \theta)$ and $V_n(r, \theta)$ are the bending moment and transverse shear respectively. Substituting equation (3) into (A1) yields

$$\begin{bmatrix} \mathrm{J}_n(k) & \mathrm{J}_n(\mathrm{i}k) & \mathrm{Y}_n(k) & \mathrm{H}_n(\mathrm{i}k) \\ \mathrm{J}'_n(k) & \mathrm{J}'_n(\mathrm{i}k) & \mathrm{Y}'_n(k) & \mathrm{H}'_n(\mathrm{i}k) \\ F_1(n, kc/a) & F_1(n, \mathrm{i}kc/a) & F_2(n, kc/a) & F_2(n, \mathrm{i}kc/a) \\ \phi_1(n, kc/a) & \phi_1(n, ikc/a) & \phi_2(n, kc/a) & \phi_2(n, \mathrm{i}kc/a) \end{bmatrix} \begin{bmatrix} A_{1n} \\ A_{2n} \\ A_{3n} \\ A_{4n} \end{bmatrix} = \begin{bmatrix} 0 \\ 0 \\ 0 \\ 0 \end{bmatrix} \tag{A2}$$

where

$$F_1(n, x) = [-n(n-1) + n(n-1)v + x^2]\,\mathrm{J}_n(x) - (1-v)x \cdot \mathrm{J}_{n+1}(x), \qquad x = \begin{cases} kc/a, \\ \mathrm{i}kc/a, \end{cases}$$

$$F_2(n, x) = \begin{cases} [-n(n-1) + n(n-1)v + x^2]\,\mathrm{Y}_n(x) - (1-v)x \cdot \mathrm{Y}_{n+1}(x), & x = kc/a, \\ [-n(n-1) + n(n-1)v + x^2]\,H_n(x) - (1-v)x \cdot \mathrm{H}_{n+1}(x), & x = \mathrm{i}kc/a, \end{cases}$$

$$\phi_1(n, x) = [-n^2(1-v) + n^3(1-v) + nx^2]\,\mathrm{J}_n(x) - [nx(1-v) + x^3]\,\mathrm{J}_{n+1}(x), \quad x = \begin{cases} kc/a, \\ \mathrm{i}kc/a, \end{cases}$$

$$\phi_2(n, x)$$

$$= \begin{cases} [-n^2(1-v) + n^3(1-v) + nx^2]\,\mathrm{Y}_n(x) - [nx(1-v) + x^3]\,\mathrm{Y}_{n+1}(x), & x = kc/a, \\ [-n^2(1-v) + n^3(1-v) + nx^2]\,\mathrm{H}_n(x) - [nx(1-v) + x^3]\,\mathrm{H}_{n+1}(x), & x = \mathrm{i}kc/a. \end{cases} \tag{A3}$$

Then, the non-trivial solution of the above equation results in

$$\begin{bmatrix} \mathrm{J}_n(k) & \mathrm{J}_n(\mathrm{i}k) & \mathrm{Y}_n(k) & \mathrm{H}_n(\mathrm{i}k) \\ \mathrm{J}'_n(k) & \mathrm{J}'_n(\mathrm{i}k) & \mathrm{Y}'_n(k) & \mathrm{H}'_n(\mathrm{i}k) \\ F_1(n, kc/a) & F_1(n, \mathrm{i}kc/a) & F_2(n, kc/a) & F_2(n, \mathrm{i}kc/a) \\ \phi_1(n, kc/a) & \phi_1(n, ikc/a) & \phi_2(n, kc/a) & \phi_2(n, \mathrm{i}kc/a) \end{bmatrix} = 0. \tag{A4}$$

By solving the characteristic equation (A4) and making use of equation (A2), the coefficients $(A_{1n}, A_{2n}, A_{3n}, A_{4n})$ can be obtained as

$$A_{1n} = -F_1(n, \mathrm{i}kc/a)|\mathrm{Y}_n(k)\,\mathrm{H}'_n(\mathrm{i}k) - \mathrm{Y}'_n(k)\,\mathrm{H}_n(\mathrm{i}k)| + F_2(n, kc/a)|\mathrm{J}_n(\mathrm{i}k)\,\mathrm{H}'_n(\mathrm{i}k) - \mathrm{J}'_n(\mathrm{i}k)\,\mathrm{H}_n(\mathrm{i}k)|$$

$$- F_2(n, \mathrm{i}kc/a)|\mathrm{J}_n(\mathrm{i}k)\,\mathrm{Y}'_n(k) - \mathrm{J}'_n(\mathrm{i}k)\,\mathrm{Y}_n(k)|,$$

$$A_{2n} = F_1(n, kc/a)|\mathrm{Y}_n(k)\,\mathrm{H}'_n(\mathrm{i}k) - \mathrm{Y}'_n(k)\,\mathrm{H}_n(\mathrm{i}k)| - F_2(n, kc/a)|\mathrm{J}_n(k)\,\mathrm{H}'_n(\mathrm{i}k) - \mathrm{J}'_n(k)\,\mathrm{H}_n(\mathrm{i}k)|$$

$$+ F_2(n, \mathrm{i}kc/a)|\mathrm{J}_n(k)\,\mathrm{Y}'_n(k) - \mathrm{J}'_n(k)\,\mathrm{Y}_n(k)|,$$

$$A_{3n} = -F_1(n, kc/a)|\mathrm{J}_n(\mathrm{i}k)\mathrm{H}'_n(\mathrm{i}k) - \mathrm{J}'_n(\mathrm{i}k)\mathrm{H}_n(\mathrm{i}k)| + F_1(n, \mathrm{i}kc/a)|\mathrm{J}_n(k)\mathrm{H}'_n(\mathrm{i}k) - \mathrm{J}'_n(k)\mathrm{H}_n(\mathrm{i}k)|$$

$$- F_2(n, \mathrm{i}kc/a)|\mathrm{J}_n(k)\mathrm{J}'_n(\mathrm{i}k) - \mathrm{J}'_n(k)\mathrm{J}_n(\mathrm{i}k)|,$$

$$A_{4n} = F_1(n, kc/a)|\mathrm{J}_n(\mathrm{i}k)\mathrm{Y}'_n(k) - \mathrm{J}'_n(\mathrm{i}k)\mathrm{Y}_n(k)| - F_1(n, \mathrm{i}kc/a)|\mathrm{J}_n(k)\mathrm{Y}'_n(k) - \mathrm{J}'_n(k)\mathrm{Y}_n(k)|$$

$$+ F_2(n, kc/a)|\mathrm{J}_n(k)\mathrm{J}'_n(\mathrm{i}k) - \mathrm{J}'_n(k)\mathrm{J}_n(\mathrm{i}k)|. \tag{A5}$$

Case 2: *Simply supported-outer, free-inner* (S–F)
In this case, the boundary conditions are

$$W_n(r, \theta) = M_n(r, \theta)|_{r=a} = 0,$$
$$M_n(r, \theta) = V_n(r, \theta)|_{r=c} = 0. \tag{A6}$$

Similar to the derivation of C–F case, one gets

$$A_{1n} = -F_1(n, \mathrm{i}kc/a)|\mathrm{Y}_n(k)F_2(n, \mathrm{i}k) - F_2(n, k)\mathrm{H}_n(\mathrm{i}k)| + F_2(n, kc/a)|\mathrm{J}_n(\mathrm{i}k)F_2(n, \mathrm{i}k)$$

$$- F_1(n, \mathrm{i}k)\mathrm{H}_n(\mathrm{i}k)| - F_2(n, \mathrm{i}kc/a)|\mathrm{J}_n(\mathrm{i}k)F_2(n, k) - F_1(n, \mathrm{i}k)\mathrm{Y}_n(k)|,$$

$$A_{2n} = F_1(n, kc/a)|\mathrm{Y}_n(k)F_2(n, \mathrm{i}k) - F_2(n, k)\mathrm{H}_n(\mathrm{i}k)| - F_2(n, kc/a)|\mathrm{J}_n(k)F_2(n, \mathrm{i}k)$$

$$- F_1(n, k)\mathrm{H}_n(\mathrm{i}k)| - F_2(n, \mathrm{i}kc/a)|\mathrm{J}_n(k)F_2(n, k) - F_1(n, k)\mathrm{Y}_n(k)|, \tag{A7}$$

$$A_{3n} = -F_1(n, kc/a)|\mathrm{J}_n(\mathrm{i}k)F_2(n, \mathrm{i}k) - F_1(n, \mathrm{i}k)\mathrm{H}_n(\mathrm{i}k)| + F_1(n, \mathrm{i}kc/a)|\mathrm{J}_n(k)F_2(n, \mathrm{i}k)$$

$$- F_1(n, k)\mathrm{H}_n(\mathrm{i}k)| - F_2(n, \mathrm{i}kc/a)|\mathrm{J}_n(k)F_1(n, \mathrm{i}k) - F_1(n, k)\mathrm{J}_n(\mathrm{i}k)|,$$

$$A_{4n} = F_1(n, kc/a)|\mathrm{J}_n(\mathrm{i}k)F_2(n, k) - F_1(n, \mathrm{i}k)\mathrm{Y}_n(k)| - F_1(n, \mathrm{i}kc/a)|\mathrm{J}_n(k)F_2(n, k)$$

$$- F_1(n, k)\mathrm{Y}_n(k)| + F_2(n, kc/a)|\mathrm{J}_n(k)F_1(n, \mathrm{i}k) - F_1(n, k)\mathrm{J}_n(\mathrm{i}k)|.$$

Case 3: *Free-outer, free-inner* (F–F)
In this case, the boundary conditions are described as

$$M_n(r, \theta) = V_n(r, \theta)|_{\substack{r=a \\ r=c}} = 0. \tag{A8}$$

Similarly, the parameters $(A_{1n}, A_{2n}, A_{3n}, A_{4n})$ are in the form

$$A_{1n} = -F_1(n, \mathrm{i}kc/a)|F_2(n, k)\phi_2(n, \mathrm{i}k) - F_2(n, \mathrm{i}k)\phi_2(n, k)| + F_2(n, kc/a)|F_1(n, \mathrm{i}k)\phi_2(n, \mathrm{i}k)$$

$$- F_2(n, \mathrm{i}k)\phi_1(n, \mathrm{i}k)| - F_2(n, \mathrm{i}kc/a)|F_1(n, \mathrm{i}k)\phi_2(n, k) - F_2(n, k)\phi_1(n, \mathrm{i}k)|,$$

$$A_{2n} = F_1(n, kc/a)|F_2(n, k)\phi_2(n, \mathrm{i}k) - F_2(n, \mathrm{i}k)\phi_2(n, k)| - F_2(n, kc/a)|F_1(n, k)\phi_2(n, \mathrm{i}k)$$

$$- F_2(n, \mathrm{i}k)\phi_1(n, k)| + F_2(n, \mathrm{i}kc/a)|F_1(n, k)\phi_2(n, k) - F_2(n, k)\phi_1(n, k)|, \tag{A9}$$

$$A_{3n} = -F_1(n, kc/a)|F_1(n, \mathrm{i}k)\phi_2(n, \mathrm{i}k) - F_2(n, \mathrm{i}k)\phi_1(n, \mathrm{i}k)| + F_1(n, \mathrm{i}kc/a)|F_1(n, k)\phi_2(n, \mathrm{i}k)$$
$$- F_2(n, \mathrm{i}k)\phi_1(n, k)| - F_2(n, \mathrm{i}kc/a)|F_1(n, k)\phi_1(n, \mathrm{i}k) - F_1(n, \mathrm{i}k)\phi_1(n, k)|,$$

$$A_{4n} = F_1(n, kc/a)|F_1(n, \mathrm{i}k)\phi_2(n, k) - F_2(n, k)\phi_1(n, \mathrm{i}k)| - F_1(n, \mathrm{i}kc/a)|F_1(n, k)\phi_2(n, k)$$
$$- F_2(n, k)\phi_1(n, k)| + F_2(n, kc/a)|F_1(n, k)\phi_1(n, \mathrm{i}k) - F_1(n, \mathrm{i}k)\phi_1(n, k)|.$$